Bioactive silk coatings reduce the adhesion of Staphylococcus aureus while supporting growth of osteoblast-like cells

Nilebäck, Linnea; Widhe, Mona; Seijsing, Johan; Bysell, Helena; Sharma, Prashant K; Hedhammar, My

Published in:
ACS Applied Materials & Interfaces

DOI:
10.1021/acsami.9b05531

ACS APPLIED MATERIALS & INTERFACES

Research Article

Cite This: ACS Appl. Mater. Interfaces 2019, 11, 24999−25007

www.acsami.org

Bioactive Silk Coatings Reduce the Adhesion of *Staphylococcus aureus* while Supporting Growth of Osteoblast-like Cells

Linnea Nilebäck,[†] Mona Widhe,[†] Johan Seijsing,[‡] Helena Bysell,[§] Prashant K. Sharma,[∥] and My Hedhammar*,[†]

[†]Department of Protein Science, School of Engineering Sciences in Chemistry, Biotechnology and Health, AlbaNova University Center, KTH Royal Institute of Technology, SE-106 91 Stockholm, Sweden

[‡]Department of Molecular Biosciences, The Wenner-Gren Institute, Stockholm University, SE-106 91 Stockholm, Sweden

[§]RISE Research Institutes of Sweden, SE-11486 Stockholm, Sweden

[∥]Department of Biomedical Engineering, University of Groningen and University Medical Center of Groningen, NL-9713AV Groningen, The Netherlands

Supporting Information

ABSTRACT: Orthopedic and dental implants are associated with a substantial risk of failure due to biomaterial-associated infections and poor osseointegration. To prevent such outcomes, a coating can be applied on the implant to ideally both reduce the risk of bacterial adhesion and support establishment of osteoblasts. We present a strategy to construct dual-functional silk coatings with such properties. Silk coatings were made from a recombinant partial spider silk protein either alone ($silk_{wt}$) or fused with a cell-binding motif derived from fibronectin (FN-silk). The biofilm-dispersal enzyme Dispersin B (DspB) and two peptidoglycan degrading endolysins, PlySs2 and SAL-1, were produced recombinantly. A sortase recognition tag (SrtTag) was included to allow site-specific conjugation of each enzyme onto $silk_{wt}$ and FN-silk coatings using an engineered variant of the transpeptidase Sortase A (SrtA*). To evaluate bacterial adhesion on the samples, *Staphylococcus aureus* was incubated on the coatings and subsequently subjected to live/dead staining. Fluorescence microscopy revealed a reduced number of bacteria on all silk coatings containing enzymes. Moreover, the bacteria were mobile to a higher degree, indicating a negative influence on the bacterial adhesion. The capability to support mammalian cell interactions was assessed by cultivation of the osteosarcoma cell line U-2 OS on dual-functional surfaces, prepared by conjugating the enzymes onto FN-silk coatings. U-2 OS cells could adhere to silk coatings with enzymes and showed high spreading and viability, demonstrating good cell compatibility.

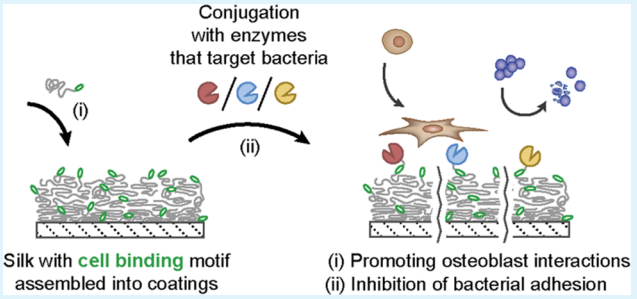

KEYWORDS: *recombinant spider silk, multifunctional coating, osseointegration, antibacterial, endolysin, Staphylococcus aureus*

INTRODUCTION

Biomaterial-associated infections (BAIs) are of great concern for implantations. Although the majority of implant surgeries are successful, the cases in which infections occur at the implants lead to suffering for the patients and high treatment costs and may result in implant failure with the consequence that the implant has to be replaced or removed.[1] Once bacteria have adhered to a surface, they produce extracellular polymeric substances to form biofilms, which provides a strong shield toward drugs, immune cells, and other environmental factors.[2,3] Implant procedures are generally accompanied by a systemic antibiotic dose to prevent biofilm formation and subsequent BAIs. The prevalence of antibiotic-resistant bacteria is however causing severe problems, being an impending global crisis.[4] According to a recent literature review, 38.7−50.9% of the microorganisms that cause postsurgery infections in the U.S. are resistant to standard prophylactic antibiotics.[5] With the most abundant pathogens in orthopedics being *Staphylococcus aureus* and coagulase-negative staphylococci,[5−7] most strains found in periprosthetic joint infections were resistant to at least one antibiotic, according to numerous clinical studies reviewed.[5] Thus, the need of alternative approaches to treat BAI is urgent, and several strategies are suggested;[8] implant surfaces can be rendered repelling to prevent adhesion of proteins and bacteria, or a local delivery of antibacterial substances can be included to provide protection. This can be achieved either by applying a drug delivery system onto the implant surface prior to insertion, followed by release of the drug in vivo, or by immobilizing active substances on the implant (e.g., for contact-killing). The effect can then remain over a longer time-period, reducing the required dose levels. Another

Received: March 28, 2019
Accepted: June 26, 2019
Published: June 26, 2019

DOI: 10.1021/acsami.9b05531
ACS Appl. Mater. Interfaces 2019, 11, 24999−25007

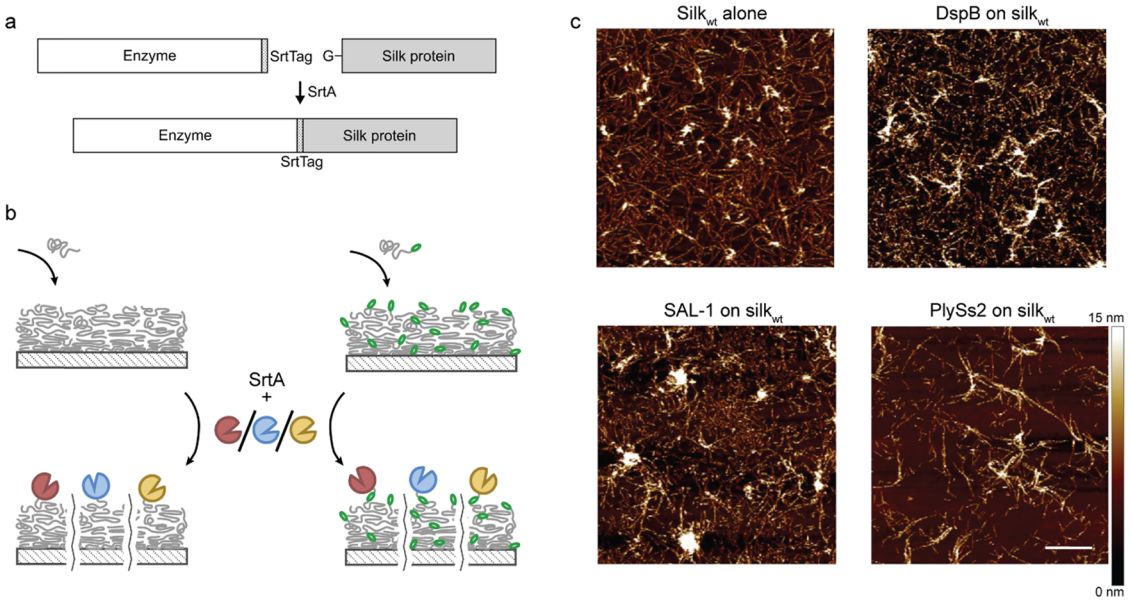

Figure 1. (a) Enzyme with the SrtTag peptide motif at the C-terminus becomes conjugated to the N-terminal glycine of the silk protein in the presence of the transpeptidase SrtA* via formation of a peptide bond between the two proteins. (b) SrtA*-mediated conjugation of various enzymes to silk can be exerted after assembly of the silk proteins into surface coatings. Two silk coating variants were used, one made from regular silk$_{wt}$ and one from FN-silk containing a cell-binding peptide motif. Three different enzymes were used separately for conjugation to silk$_{wt}$ or FN-silk, in the latter case giving rise to dual-functional coatings. (c) Atomic force microscopy (AFM) images showing morphology of silk coatings with and without conjugated enzymes. For better contrast of fibrils, the height scale has been adjusted to show variations within 15 nm. Maximum height ranges were 18.6 nm for silk$_{wt}$ alone, 26.6 nm for DspB on silk$_{wt}$, 29.4 nm for SAL-1 on silk$_{wt}$, and 16.1 nm for PlySs2 on silk$_{wt}$. Scale bar represents 1 μm.

approach is to disrupt the polymeric substances in the biofilm matrix.[9] This strategy does not kill bacteria but might be a sustainable option since it makes the bacteria susceptible to other drugs and the immune system. It has been suggested that multifunctional implant modifications are essential to achieve long-lasting and effective BAI prevention, and therefore evaluation of several of the above-mentioned strategies is of importance.[1,10]

Enzymes that target bacteria or biofilm matrix components will broaden the cohort of antibacterial substances in use. A major point to consider when constructing catalytically active surfaces is that the enzymes are dependent on a proper fold to be able to perform their action. Thus, mild conditions are needed during the preparation procedure. We have previously described a method to prepare stable silk coatings from a recombinant spider silk protein called 4RepCT by utilizing its self-assembling properties.[11] Under physiological-like conditions, these silk proteins assemble into thin nanofibrillar coatings, also after fusion with different functional peptides (i.e., cell-binding motifs and antimicrobial peptides)[11−13] and fold-dependent domains (i.e., growth factors and affinity domains)[14,15] using recombinant gene technology. To functionalize silk with larger proteins such as enzymes, we present a strategy for site-specific immobilization of enzymes with a short sortase recognition peptide motif (SrtTag) in mild buffer onto preassembled silk using an engineered variant of the transpeptidase Sortase A.[16] This results in a peptide bond between the silk coating and the respective enzyme (Figure 1a).

Two endolysins were chosen for their bactericidal properties, and one enzyme was chosen for its ability to disperse biofilms. Endolysins are enzymes encoded by bacteriophages, which are produced at the end of their infection cycle to lyse their bacterial host from the inside.[17,18] The endolysins degrade the peptidoglycans of the cell wall, causing leakage to spread the replicated phages. Their potential as therapeutics has recently started to be explored in the clinic.[19] In this work, we used the endolysins PlySs2 and SAL-1. PlySs2 has been identified from a prophage region in the genome of *Streptococcus suis* isolates. It was shown to efficiently lyse several streptococcal and staphylococcal strains, including methicillin-resistant *S. aureus* (MRSA).[20] It has also been used to reduce *S. suis* colonization in a murine in vivo nasal mucosa model.[21] SAL-1 was isolated from the bacteriophage SAP-1 and has been shown to lyse several staphylococcal strains including MRSA. Its safety and pharmacokinetics were evaluated in a phase 1 clinical study with healthy adults, where it showed only mild adverse effects, making it promising for further clinical trials.[22]

Dispersin B (DspB) is a glycoside hydrolase produced by *Aggregatibacter actinomycetemcomitans* to regulate its biofilm colonization.[23] It can potentially be used to prevent BAI by releasing bacteria from biofilms, thus making them accessible for the immune response or other bactericidal substances. DspB cleaves polymeric β-1,6-*N*-acetyl-D-glucoseamine (poly-β-1,6-NAGA), a polymer that is synthesized by microbes possessing genetic loci homologous to the *pgaABCD* and *icaABCD* operons of *E. coli* and staphylococci, respectively.[24]

In addition to harboring antibacterial and antibiofilm properties, an orthopedic implant surface should ideally promote osteoblasts to adhere to and cover the surface. During the initial time after implantation, a limited interaction with bacteria would reduce the risk of bacterial colonization and, in that way, instead give opportunities for osteoblasts to establish on the surface. To promote fast establishment of mammalian cell interactions at the surface, we used a silk

DOI: 10.1021/acsami.9b05531
ACS Appl. Mater. Interfaces 2019, 11, 24999−25007

protein variant containing a cell-binding motif from fibronectin, called FN-4RepCT, as the base for the surface coatings. FN-4RepCT has previously been shown able to promote adhesion of mesenchymal stem cells, fibroblast, endothelial cells, and keratinocytes, as well as smooth muscle cells.[12,25,26] In this work, we conjugated antibacterial and antibiofilm enzymes onto silk coatings made of either wild-type 4RepCT ($silk_{wt}$) or FN-4RepCT (FN-silk) (Figure 1b). The latter variant thus provides dual functions, with potential to both prevent bacterial adhesion on the implant and promote tissue integration. The outcome was studied by letting *S. aureus*, a relevant pathogen in orthopedic implant infections, adhere to the coatings and observing the number of live and dead bacteria using fluorescence microscopy. Moreover, an osteosarcoma cell line was used as a model for osteoblasts and cultured on the coatings for assessment of cell compatibility by studying initial adhesion as well as viability over several days.

EXPERIMENTAL SECTION

Proteins. Two silk proteins were used: the recombinant partial spider silk protein 4RepCT (23 kDa), herein referred to as wild-type silk ($silk_{wt}$), and a variant containing an RGD-loop derived from fibronectin, called FN-4RepCT (25 kDa, FN-silk). Both silk proteins have been described elsewhere.[12,27] The silk proteins were produced recombinantly and were generously provided by Spiber Technologies AB. Silk proteins were sterile-filtered (pore size 0.2 μM) and stored frozen in 20 mM tris(hydroxy-methyl)aminomethane (Tris) buffer, pH 8.0, until use.

A vector containing the gene for the Sortase A variant used in this work was received as a kind gift from Dr. Kristina Westerlund. This variant has three mutations (P94S, D160N, K196T) for enhanced efficiency compared with wild-type Sortase A, being evolved by Chen et al. using yeast display,[28] and lacks the membrane anchoring domain.[16] The mutated variant is hereafter denoted SrtA*. It catalyzes a reaction between the SrtTag peptide added to each enzyme and the N-terminal glycine of $silk_{wt}$ or FN-silk. SrtA* was expressed recombinantly and purified as previously described.[16]

The sequence of DspB was derived from PDB-ID 1YHT with the following adaptations: a His_6-tag was placed N-terminally, and nonstructured linkers were added preceding an LPETGG motif (SrtTag) at the C-terminus (GSSG-H_6-1YHT-GSG-PAAL-GSAS-$(GS)_3$-LPETGG). The resulting protein was 44 kDa. The sequence of PlySs2 was adapted from the GenBank sequence AME89909.1 by adding linkers, the SrtTag and a His_6-tag at the C-terminus (AME89909-GSSG-PAAL-GSSG-LPETG-H_6), resulting in a 28 kDa protein. The sequence of SAL-1 was derived from the GenBank sequence AFN38718.1 with three amino acids exchanged (V26I, E113Q, Q485H)* as acquired from Jun et al.,[29] with addition of linkers, the SrtTag and a His_6-tag at the C-terminus (AFN38718.1*-GSSG-PAAL-GSSG-LPETG-H_6), for a total size of 57 kDa.

Enzymes were produced recombinantly in *Escherichia coli* BL21* (DE3). After cultivation at 150 rpm, 37 °C, endolysin cultures were cooled on ice before addition of the inducer agent isopropyl-β-D-thiogalactopyranoside (0.5−1 mM). Harvesting was done after overnight expression at 150 rpm, ambient temperature, by centrifugation at 7000*g*, 4 °C for 10 min. Pellets were resuspended in 50 mM Tris/300 mM NaCl/30% glycerol/10 mM imidazole (pH 8.0) and saved at −20 °C. A similar protocol was followed for production of DspB, for which overnight expression instead was performed at 25 °C, and the harvest pellet was resuspended in 20 mM Tris/200 mM NaCl (pH 8.0). Prior to purification, cell suspensions were thawed and lysed by sonication at 35% amplitude with pulses of 1.0 s of run and 1.0 s of rest, for a run time of 1.5 min. Lysates were centrifuged at 10 000*g*, 4 °C for 30 min. Supernatants of SAL-1 were incubated with 8.8 U/mL DNaseI and 1.7 μL/mL $MgCl_2$ (1 M) for 30 min to reduce the suspension viscosity. Whereas DspB could be applied to prepacked Ni-NTA columns equilibrated with the DspB lysis buffer, endolysins were kept in a high glycerol content to reduce stability issues and were thus preincubated with 1 mL of Ni-NTA resin each. Resin and lysate mixes were rotated at 4 °C for 2 h and were subsequently packed into gravity flow chromatography columns. Columns were washed with low imidazole concentration and eluted in 20 mM Tris/200 mM NaCl/200 mM imidazole for DspB and 20 mM Tris/300 mM NaCl/30% glycerol/250 mM imidazole for SAL-1 and PlySs2. Purity was confirmed using sodium dodecyl sulfate polyacrylamide gel electrophoresis (SDS-PAGE). Proteins were sterile-filtered and stored at ∼8 °C, and samples containing glycerol were kept on ice.

Enzymatic Activity Assays. The lytic activities of purified SAL-1 and PlySs2 were assessed by monitoring the reduction in optical density (OD_{600}) of *S. aureus* SA113 during 100 min. Aliquots of *S. aureus* were prepared by cultivation in tryptic soy broth (TSB) at 37 °C, 150 rpm and harvested during the log phase at OD_{600} = 0.4. The pellets were washed and resuspended in 10 mM phosphate/150 mM NaCl/25% glycerol, pH 7.5 to 1:10 of the cultivation volume for storage at −80 °C. Right before the experiment, an aliquot was thawed and diluted until OD_{600} = 2. A total volume of 100 μL per well was prepared in 96-well plates by addition of bacteria to endolysin solutions, to achieve final concentrations of 25, 50, or 100 nM of either SAL-1 or PlySs2 per well and OD_{600} = 1 of *S. aureus*. Then, 100 μL of *S. aureus* at OD_{600} = 1 was added to wells with silk coatings prepared as described below as negative controls. Each sample type was prepared in triplicates, and the optical density was monitored in a Polar Star Omega plate reader (BMG Labtech) at 595 nm, with 200 rpm orbital shaking before each cycle and 200 rpm meander corner shaking between cycles.

The catalytic ability of purified DspB was assessed by incubation with an analogue for its natural substrate poly-β-*N*-acetyl-D-glucosamine. Upon enzymatic cleavage of the glycosidic linkage in 4-nitrophenyl-*N*-acetyl-β-D-glycosaminide (NP-NAGA, Sigma-Aldrich), formation of 4-nitrophenolate can be monitored by absorbance at 405 nm. A dilution series of soluble DspB in 50 mM phosphate buffer at pH 7.0 was prepared and mixed with a freshly prepared stock solution of NP-NAGA to obtain the concentration range 75−250 nM of DspB in 2 mg/mL NP-NAGA. The conversion to the colorimetric product was measured in a ClarioSTAR plate reader (BMG Labtech) at 405 nm after addition of a base to deprotonate the product. For this, 10 μL of 1 M NaOH was added to reaction volumes of 100 μL at 72 h after the reaction start. Samples were prepared in triplicates. The catalytic ability of immobilized DspB on silk coatings, prepared as described in the Method subsection below for functionalization, was monitored after addition of 2 mg/mL NP-NAGA in 50 mM phosphate buffer at pH 7.0, as described above. Samples were prepared in duplicates in six experimental replicates.

Silk Coatings Functionalized with Enzymes. First, 200 μL drops of silk solutions (0.1 g/L $silk_{wt}$ or FN-silk in 20 mM Tris) were placed in the middle of wells of 12-well suspension plates (Greiner CellStar Bio-One) to prepare coatings for bacterial adhesion. After 1 h incubation at ambient temperature, drops were removed, and the resulting surface coatings were washed three times with 200 μL of 20 mM Tris. Coatings were stored dry at ambient temperature. The same procedure was used to prepare silk coatings for U-2 OS culturing, using 60 μL of silk solutions to cover the whole bottoms in 96-well suspension plates (Sarstedt) and 60 μL of 20 mM Tris for washes. All coatings were made under sterile conditions.

To functionalize silk coatings ($silk_{wt}$ or FN-silk) with SAL-1, PlySs2, or DspB (containing the SrtTag), reaction mixtures were prepared with 3 μM SrtA* and 4.3 μM of respective enzyme-SrtTag in a sortase ligation buffer (50 mM Tris, 150 mM NaCl, 10 mM $CaCl_2$, pH 7.5). Then, 60 or 100 μL of the reaction mixture was added to silk coatings in multiwell plates for cell cultures or bacterial cultures, respectively, and SrtA*-mediated conjugation was allowed to proceed at ambient temperature. After 2 h, reaction mixtures were removed, and coatings were washed three times with 60 or 100 μL of phosphate-buffered saline (PBS) separately. This functionalization was made under sterile conditions just before starting bacterial adhesion trials or U-2 OS culturing on silk coatings.

DOI: 10.1021/acsami.9b05531
ACS Appl. Mater. Interfaces 2019, 11, 24999−25007

The maximum theoretical number of enzymes conjugated to silk coatings was calculated as follows. From a quartz crystal microbalance with dissipation and ellipsometry data presented by Nilebäck et al.,[11] the adsorbed mass of silk proteins was monitored as a function of time during surface assembly into silk coatings. After 60 min of adsorption using a solution of 0.1 g/L silk proteins, as used in this work, the total mass of silk proteins in the coating, including 77% water, was 2.0 μg/cm^2, so that the dry mass can be assumed to be 0.46 μg/cm^2. Given the molecular weight of silk being 23 350 Da, the molar amounts of silk in such a coating would be 20 pmol/cm^2. Upon maximum efficiency of the SrtA*-mediated conjugation, one enzyme (DspB, SAL-1, or PlySs2) can be conjugated to each silk protein. Thus, the maximum theoretical number of enzymes in the silk coatings after conjugation is estimated to be 20 pmol/cm^2.

The morphology of silk coatings, prepared as described above, was evaluated using atomic force microscopy (AFM). Height images were obtained for samples in a droplet of PBS buffer using ScanAsyst Fluid + cantilevers (Bruker) for PeakForce tapping in a FastScan instrument (Bruker). Imaging was made using 20 nm amplitude and a setpoint of 600 pN.

Bacterial Adhesion onto Coatings. First, 10 mL of tryptic soy broth (TSB) was inoculated with a single colony of *S. aureus* 12 600 from an agar plate and incubated at 37 °C under static conditions for 24 h. The preculture was poured into 200 mL of TSB and cultured at 37 °C under static conditions for 16 h. Bacteria were harvested by centrifugation at 6500*g* at 10 °C for 5 min. Bacteria were washed twice by resuspending the pellet in 10 mL of PBS and repeating the centrifugation step. After a third resuspension, bacterial aggregates were dispersed by sonication on ice using 30 cycles of 1 s drive and 2 s rest at 60% amplitude. Bacteria were counted in a Bürker-Türk chamber and diluted to 3 × 10^8 bacteria/mL in PBS.

Then, 2 mL of bacterial solution was added per well in 12-well plates where silk coatings had been prepared with or without conjugating enzymes onto them. The plate was incubated at 37 °C, 60 rpm during 1 h to let bacteria adhere to samples. Bacterial suspensions were removed, and coatings were washed once with 2 mL of PBS by slow and gentle pipetting. Coatings were covered with live/dead stain (BacLight, Invitrogen) and incubated in the dark for 15 min. After removing the stain, 2 mL of PBS per well was gently added, and samples were imaged using a Leica DM4000B fluorescence microscope with the HCX APO L 40×/0.80 W objective, excitation filters BP 470/50 nm and BP 515−560 with dichromatic mirrors 500 and 580 nm, for green and red stain, respectively. The number of bacteria from the green and red channels, respectively, was counted from captured images with the size area 0.00037688 cm^2. The percentage of mobile bacteria was estimated visually for each imaged area. For at least five positions within the camera view, the number of mobile bacteria within groups of ten neighboring bacteria was counted and averaged with 5% precision. Time-lapse captures were done in a Leica TCS SP2 confocal microscope with an HCX APO L 63×/0.9 W objective, argon laser at 488 nm with emission filter 500−550 nm, HeNe laser at 543 nm with emission filter 555−725 nm and 3 s between each frame. ImageJ (version 2.0.0) was used to generate compiled images by averaging the intensity in each pixel from 41 subsequent captures in time-lapses. To remove loosely adhered bacteria, plates were incubated in an orbital shaker at 25 °C, 120 rpm for 10 min after the first imaging. The liquid was exchanged to clean PBS before imaging again. The number of experimental replicates was N = 3−13 (silk$_{wt}$ = 13, SAL-1-silk = 3, PlySs2-silk = 8, DspB-silk = 3, FN-silk = 11, SAL-1-FN-silk = 8, PlySs2-FN-silk = 8, DspB-FN-silk = 8) for regular counts with n = 3−10 images per individual sample (n_{median} = 5), N = 4 for mobility, and N = 5 for washing tests with n = 3−6 images per individual sample (n_{median} = 4).

Human Osteosarcoma U-2 OS Cell Culturing. U-2 OS (ATCC HTB-96) were cultivated in McCoy's 5A Modified Medium (Sigma) supplemented with 10% fetal bovine serum (Sigma), at 37 °C with 5% CO_2 and 95% humidity. Silk coatings with or without enzymes were prepared in 96-well suspension plates as described above. Empty wells of suspension plates or 96-well tissue culture treated (TCT) plates (Nunclon Delta, Thermo Scientific) were used as controls. For assessment of cell adhesion to silk coatings, 10 000 cells/well were added, and plates were placed in the incubator for 1 h. After this, cell suspensions were removed, each well was washed twice with PBS, and cells were fixed with 99.5% ethanol for 10 min. Wells were then washed three times with deionized water. Cells were stained with 0.1% crystal violet in water for 30 min, followed by four washes with deionized water. Wells were dried overnight and imaged in an inverted bright field microscope. For quantification, the stain was dissolved by adding 40 μL of 20% acetic acid per well and incubating the plates at a shaking table for 30 min. Thereafter, 35 μL/well was moved to a 384-well plate, and absorbance was read in a CLARIOstar plate reader (Bmg Labtech) at 595 nm. Blanks were made by staining empty wells in the suspension culture plate and wells preincubated with medium in the tissue culture treated plate. The corresponding blank was subtracted from sample values according to their plate type. Viability of cells was assessed by seeding of 2000 cells/well at day 0. At days 1, 4, and 7, the culture medium was removed, and Alamar Blue cell viability reagent (Invitrogen, 1:10 dilution in culture medium) was added. Plates were placed in the cell incubator for 2 h. Supernatants were used for fluorescence readout in a CLARIOstar plate reader at $\lambda_{excitation}$ = 540 nm and $\lambda_{emission}$ = 595 nm. Alamar blue in a medium without cells was used as the blank and subtracted from the measurement values. Both assays were performed three times with quadruplicate wells (N = 3, n = 4).

Statistical Analysis. Standard deviations were calculated for each sample. For bacterial counts and crystal violet staining of osteosarcoma cells (i.e., for data where technical replicates were merged into one data set), error propagation was performed to obtain the standard deviation per sample type. For the Alamar blue cell viability assay, statistical analyses were performed on each technical replicate, and the most representative experiment is shown. One-way analysis of variance was conducted in GraphPad Prism for bacterial counts, crystal violet quantifications, and Alamar blue viability assay, with following multiple comparisons of means using Tukey's test. For bacterial counts and mobility percentages in wash experiments, paired *t*-tests were done for the difference before and after wash for each sample type.

RESULTS AND DISCUSSION

Characterization of the Enzymes and Coatings. All recombinantly produced proteins were purified using immobilized metal ion affinity chromatography. SDS-PAGE analysis confirmed high purity of proteins of expected sizes (SrtA* somewhat bigger than 24 kDa) (Figure S1).

Further, the catalytic ability of the produced enzymes in solution was confirmed in two different assays. For SAL-1 and PlySs2, their ability to lyse *S. aureus* was confirmed in a turbidity reduction assay. PlySs2 could reduce the optical density of bacterial suspension at 100 nM (2.8 μg/mL), whereas SAL-1 was effective in concentrations down to 25 nM (1.4 μg/mL) (Figure S2). Previously, minimal inhibitory concentrations (MIC values) toward various substrains of *S. aureus* were reported to be 16−32 μg/mL for PlySs2[20] and 0.22−3.24 μg/mL for SAL-1.[29] Thus, the recombinantly produced endolysins used herein possessed catalytic potency in similar concentration ranges as what has been previously reported.

The third enzyme used in this project, DspB, has the ability to degrade the NAGA polymer in biofilms from certain strains. Characterization of the catalytic ability of DspB after recombinant production was made using a substrate analogue that is converted to a colorimetric product upon cleavage of a glucosidic linkage by DspB. A linear correlation between concentration and activity was observed, and DspB conjugated to silk coatings using SrtA* showed readouts corresponding to

DOI: 10.1021/acsami.9b05531
ACS Appl. Mater. Interfaces 2019, 11, 24999−25007

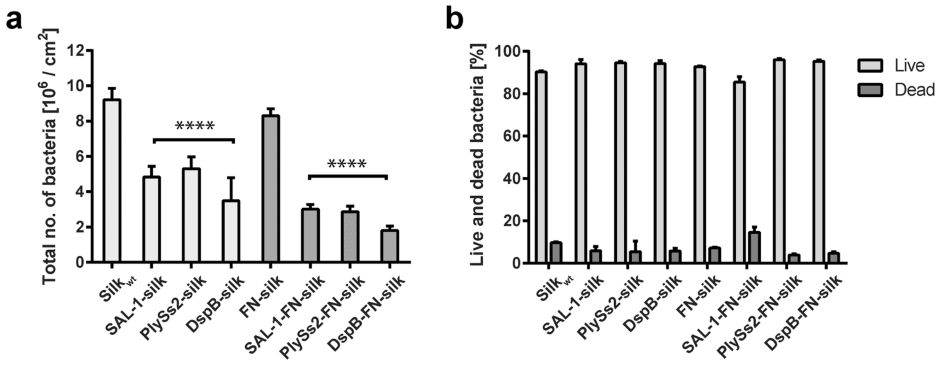

Figure 2. Bacterial counts after 1 h adhesion on silk coatings. (a) Total number of bacteria, and (b) the percentage of live and dead bacteria, respectively, of the total count. Statistical significance levels are shown related to the respective silk control, ****$p < 0.0001$.

soluble DspB at concentrations in the nanomolar range (Figure S3).

The silk coatings used herein are formed by self-assembly of 4RepCT silk proteins in mild aqueous buffers onto hydrophobic solid substrates, where the proteins are structurally rearranged into β-sheet-rich, nanofibrillar structures.[30] The coatings have been shown stable toward wash with 0.5 M hydrochloric acid, 0.5 M sodium hydroxide, and 70% ethanol, and it is hypothesized that the stability is enabled by the structure optimization that occurs during the silk assembly.[11,30] The thickness of the coatings depends on the concentration of the silk protein solution as well as the time for assembly. From previous QCM-D and ellipsometry data, it is estimated that the coating procedure typically results in 20 nm-thick coating, corresponding to 0.46 μg silk per cm^2.[11,31] The silk coatings have a high wettability and are thus hydrophilic, typically resulting in complete spreading of a water droplet (i.e., contact angle measurements not applicable). The high wettability was retained after conjugation of DspB, SAL-1, or PlySs2 to the silk coatings. The nanofibrils in the silk coatings are 8−20 nm in diameter for unconjugated silk coatings.[11] Similar nanofibrillar morphologies were observed for silk coatings also after SrtA*-mediated conjugation with DspB, SAL-1, or PlySs2 (Figure 1c). The maximum theoretical number of enzymes obtained on the final silk coatings is 20 pmol/cm^2 (see the Experimental Section for calculations), but the real number is likely a lot less, since the coupling efficiency is not 100%.

Enzymes Conjugated on Silk Coatings Leads to Reduced Bacterial Adhesion. The number of adhered bacteria was reduced on all silk coatings conjugated with enzymes, compared with respective silk controls ($p < 0.0001$) (Figure 2a). There were no significant differences among the three enzyme variants when compared within the same silk group (conjugation onto silk$_{wt}$ or FN-silk coatings, respectively). Despite the reported capacity of *S. aureus* to bind fibronectin,[32] bacterial adhesion to FN-silk was not enhanced compared with silk$_{wt}$. This is in agreement with previous studies showing that the fibronectin adhesive proteins of *S. aureus* bind to fibronectin at sites separated from the RGD-loop. In vivo, this allows simultaneous binding of tissue cells to the RGD-loop, resulting in a fibronectin bridging that allows the bacterium to invade the host cell by internalization.[33] By using only the RGD-loop in the FN-silk to aid adhesion of mammalian cells, and excluding other parts of fibronectin from the silk coatings, this mechanism is bypassed. In fact, bacterial counts were lower on all FN-silk coatings than on silk$_{wt}$ coatings at the significance level $p < 0.01$ or less.

Although the bacterial adhesion was significantly lower to silk coatings after conjugation with enzymes, implying that they have an impact on the bacteria, viability staining of *S. aureus* after 1 h incubation on silk coatings revealed that >85% of the adhered bacteria were alive on all coatings irrespective of the total counts (Figure 2b). The function of DspB is to degrade an extracellular polymer in the biofilm matrix rather than killing the bacteria. SAL-1 and PlySs2, on the other hand, should lyse *S. aureus* by degrading the peptidoglycans in the cell wall, and thus a lower degree of live bacteria would be expected on those samples. Possibly, complete lysis occurs only if the bacterium stays close to the immobilized SAL-1 and PlySs2 long enough for a significant disruption of the peptidoglycan to occur. In this case, it might be that the enzyme cleaves off the bacterium as soon as it approaches the surface, thus releasing it before the enzyme has time to degrade a sufficient portion of the peptidoglycan to kill the bacterium. The effect will then be antiadhesive rather than bactericidal. The amount of bacteria added to the samples was deliberately high to give a fair coverage of the large natural variation that occurs when using fresh bacterial cultures for each experimental replicate. Therefore, a noticeable amount of bacteria was found also on coatings with enzymes. Still, a significant reduction in adhesion levels was obtained, which reduces the risk of bacterial colonization and subsequent biofilm formation. The effect would probably be even more pronounced in real scenarios, where the amount of bacteria that challenges the implant is much lower.

Since lower bacterial counts were observed on coatings when enzymes were immobilized on FN-silk compared with immobilization on silk$_{wt}$ coatings (Figure 2), and since dual-functional coatings are obtained when using FN-silk, subsequent experiments were conducted on FN-silk coatings conjugated with SAL-1, PlySs2, and DspB, with FN-silk and silk$_{wt}$ as controls.

Bacteria are Mobile on Silk Coatings with Immobilized Enzymes. Under the microscope, the bacteria were observed to be more mobile on silk coatings with enzymes than on the control surfaces. The mobility seemed to be partially restricted, causing the bacteria to move around an attachment point, with rotation radius several times larger than the size of a bacterium. Example videos of time-lapse captures that were taken every third second using the green emission channel, showing live bacteria, can be found as the Supporting Information (Video S1: PlySs2 on silk$_{wt}$; Video S2: silk$_{wt}$ control). From the time-lapse captures, a compiled image was obtained by averaging the intensity in each pixel over 41

DOI: 10.1021/acsami.9b05531
ACS Appl. Mater. Interfaces 2019, 11, 24999−25007

frames (120 s). The influence of mobile bacteria is diminished in the averaged image, whereas firmly adhered (nonmobile) bacteria are still clearly visible. The effect is seen in Figure 3,

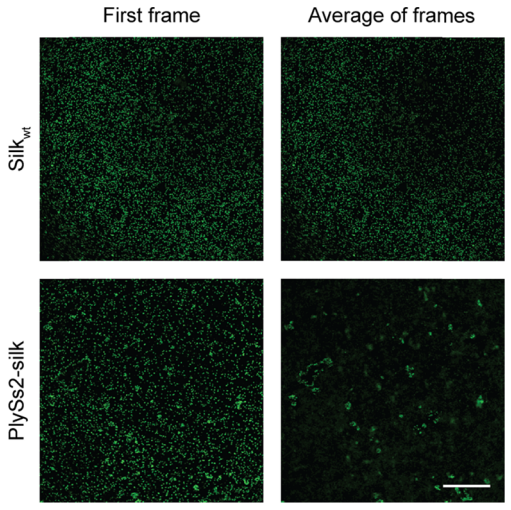

Figure 3. Frames from time-lapse series tracking the mobility of live bacteria at the surface of silk$_{wt}$ (top panel) and PlySs2-silk (bottom panel) coatings. The first frame from each time-lapse series is shown in the left lane. The images in the right lane are averages of the intensity in each pixel for 41 frames in the time-lapse. Scale bar represents 50 μm.

where the first frame of the time-lapse series is shown next to the averaged frame, for silk$_{wt}$ and PlySs2-silk coatings. The first frame thus represents all bacteria, both mobile and nonmobile. While most bacteria on the silk$_{wt}$ coating are seen in both images with similar intensities, the averaged image of PlySs2-silk has a markedly lower amount of intense bacteria compared with the single frame, which is an effect of a large number of mobile bacteria. The percentage of mobile bacteria was assessed manually during microscopy and was found to be higher on all silk coatings with enzymes than on control coatings ($p < 0.001$). The highest percentage of mobile bacteria was seen on FN-silk coatings with DspB (83%), followed by coatings with PlySs2 (71%) and SAL-1 (53%). Noteworthy, bacteria on polystyrene and glass controls showed high counts but no mobility ($\ll$1%). Similarly, most bacteria on silk$_{wt}$ and FN-silk controls were firmly adhered, but a certain ratio of mobility was observed (10 and 13%, respectively). One hypothesized cause to the mobility could be that some silk fibrils in the coatings have a flexible end that moves due to Brownian motion, bringing bacteria that have adhered to that end to join the movements. The markedly higher numbers of mobile bacteria on coatings with enzymes can however not be explained by this, but are more likely caused by incomplete or ongoing detachment caused by the enzymes.

Different washing protocols were tried, and upon rotation of the plate at 120 rpm in an orbital shaker, the main portion of mobile bacteria was detached and washed off, leaving 5−10% mobile bacteria on silk$_{wt}$, FN-silk, and SAL-1-FN-silk, 16% on PlySs2-FN-silk, and 19% on DspB-FN-silk (Figure 4a). Washing resulted in reduced numbers for all samples types, and the bacterial counts after washing were the lowest on PlySs2-FN-silk and DspB-FN-silk (Figure 4b). The fact that mobile bacteria were removed by the wash protocol makes it reasonable to hypothesize that their adhesion is less strong than the adhesion of the bacteria that were motionless on the coatings. The bacterial adhesion forces could for example be further studied by bacterial vibration spectroscopy, as has been shown by Song et al.,[34] although this is cumbersome. It is hard to simulate a real situation to assess the implication of this, also because of the complexity of exerted forces at different positions of the coatings in the multiwell plate upon rotation. However, a weaker adhesion and the possibility to detach bacteria upon washing indicate that DspB, as well as SAL-1 and PlySs2, can provide a function to implant surfaces by keeping the number of strongly adhered bacteria at the surface low.

Some other parameters may have influenced the surface properties, although they are difficult to investigate. The amount of enzymes on surfaces is hard to determine and was solely controlled by the molar ratios used during the sortase-mediated reaction. The surfaces were washed carefully after the coupling reaction, but it is possible that unspecifically bound enzymes or sortase were still present on the surfaces during the assays.

Osteosarcoma Cells Adhere to and Grow on Silk Coatings with Enzymes. The osteosarcoma cell line U-2 OS was used as a model for studying osteoblast compatibility of the coatings. First, the ability of U-2 OS cells to adhere to silk coatings and controls during 1 h was assessed by microscopy. A clear improvement in the capability of U-2 OS to quickly adhere to FN-silk was observed, compared with silk$_{wt}$ as well as both types of bare culture plates (the hydrophobic plate, HP,

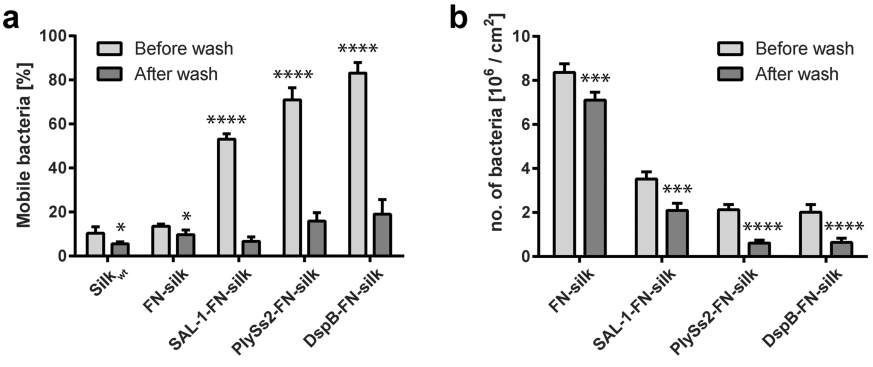

Figure 4. (a) Ratio of mobile bacteria on surfaces and (b) total number of live and dead bacteria on silk coatings before (light gray) and after (dark gray) wash at 120 rpm. Statistical significance levels are shown for comparisons of values before and after wash, *$p < 0.05$, **$p < 0.01$, ***$p < 0.001$, ****$p < 0.0001$.

DOI: 10.1021/acsami.9b05531
ACS Appl. Mater. Interfaces 2019, 11, 24999−25007

in which the silk coatings were made, and the tissue culture treated plate, TCT) (Figure 5). Cells could spread better on

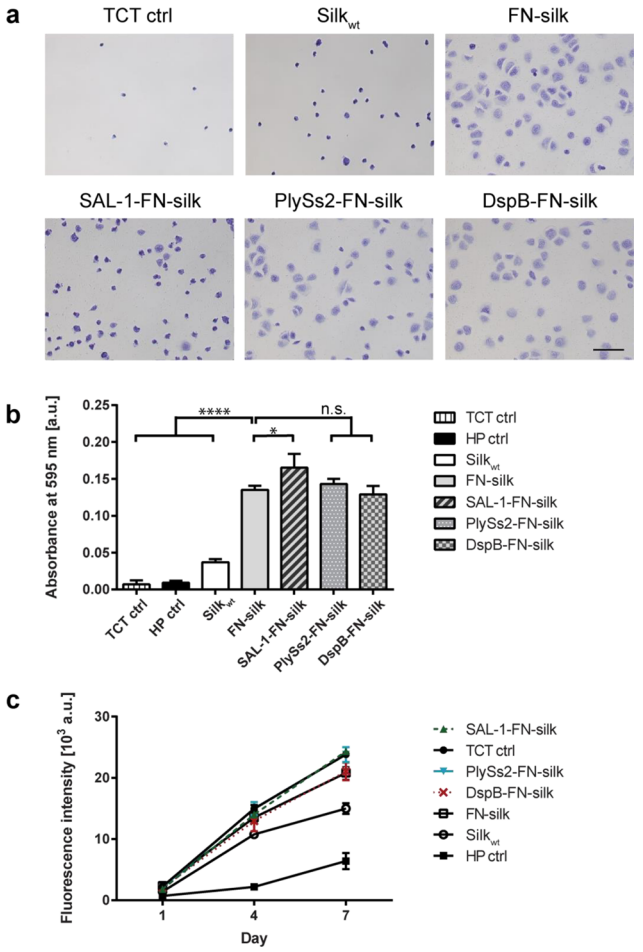

Figure 5. (a) Morphology of U-2 OS cells after 1 h adhesion, at 20× magnification. The scale bar represents 100 μm. (b) Quantification of cell stainings after 1 h adhesion. Statistical significance levels are shown for comparisons with FN, ns = no significance, *$p < 0.05$, ****$p < 0.0001$. (c) Alamar blue viability assay over 7 days of U-2 OS culturing. FN-silk and silk$_{wt}$ were used as silk controls, and bare hydrophobic plate (HP) and tissue culture treated (TCT) wells were used as standard controls. A representative replicate out of triplicate experiments is shown, with the legend sorted according to the values at day 7.

FN-silk than on both plate controls, an ability that was maintained also in the presence of enzymes in the FN-silk coatings with PlySs2 or DspB (Figure 5a). The cells on FN-silk coatings with SAL-1 had a slightly less spread-out shape, although the quantification of the stain that was dissolved after microscopy showed similar levels for FN-silk with SAL-1 as for the other FN-silk variants (Figure 5b), with slightly higher values for SAL-1-FN-silk than for DspB-FN-silk and FN-silk alone ($p < 0.05$), but no statistical difference between SAL-1-FN-silk and PlySs2-FN-silk. Thus, the number of cells adhering to the silk coatings was not inhibited by the enzymes. All FN-silk variants had higher values than silk$_{wt}$, as well as HP and TCT controls ($p < 0.0001$).

Viability of the adhered cells was assessed by quantifying the metabolic activity after 1, 4, and 7 days of culture (Figure 5c). A high total metabolic activity was observed for adhered cells on all FN-silk coatings, including those conjugated with enzymes, with similar levels as for culturing on the bare TCT plate. They showed higher values than cells on silk$_{wt}$ coatings ($p < 0.05$ or lower), which in turn had elevated numbers compared with the bare HP plate ($p < 0.001$). The experiments show that the osteoblast-like cell line has good viability and grow well also in the presence of the surface-bound antibacterial or antibiofilm enzymes SAL-1, PlySs2, and DspB.

The maintained cytocompatibility of silk coatings after conjugation with the enzymes SAL-1, PlySs2, and DspB suggests that these coatings can be used to prevent bacterial adhesion without having an adverse influence on osseointegration. Instead, the advantage of having FN-silk as a base coating is retained also after sortase-mediated conjugation with enzymes. This was seen in both the cell adhesion and cell viability assays. The presence of the RGD-loop in FN-silk coatings with enzymes is clear, especially when looking at the initial cell adhesion during the first hour of U-2 OS culture. Culture of keratinocytes on FN-silk has previously been shown to result in significantly higher formation of focal adhesions, compared with silk$_{wt}$.[12] Integrin $\alpha_5\beta_1$ was detected in the binding of keratinocytes to FN-silk, suggesting specific integrin−fibronectin binding as the mechanism behind the improved cell adhesion to FN-silk as compared with silk$_{wt}$.[12] In this work, all FN-silk coatings outcompeted both types of bare cell culture plates, with faster adhesion, as well as better spreading. The reduced or delayed cell spreading on FN-silk with SAL-1 may be due to a potentially higher amount of surface-bound enzymes compared with coatings with PlySs2 and DspB or may be an effect of other molecular properties (e.g., size, fold, hydrophilicity, or other characteristics). However, the overall cell compatibility of FN-silk with SAL-1 is satisfactory since the amount of adhered cells and subsequent proliferation pattern is comparable to the other FN-silk coatings according to quantification both after 1 h adhesion and after 4 and 7 days of culturing (Figure 5b,c).

Potentials of Multifunctional Silk Coatings. By using a coating that simultaneously reduces bacterial adhesion and allows osteoblast-like cells to adhere and spread on the surfaces already during the first hour after implantation, the balance can be pushed toward better osseointegration. This in turn may contribute to an environment that promotes healing and allows the immune response to target the bacteria that still adheres to the surface, as well as those in the surrounding. The competition between biomaterial-associated infection and tissue integration was presented several decades ago by Gristina[35] and is referred to as "the race for the surface". However, most research efforts still focus only on one of these aspects at a time. In this work, we used dual-functional coatings and could confirm both properties individually for SAL-1-FN-silk, PlySs2-FN-silk, and DspB-FN-silk. For future studies, cocultivation of bacteria and cells is of interest, an indeed intriguing and delicate task to undertake. Such an approach has already been neatly investigated in initial studies with promising results.[36,37] During a surgical procedure, the number of bacteria that an implant surface is challenged with has been estimated at 270 cm^{-2},[36] which is a factor 10^{-4} less than what we observed on our silk$_{wt}$ and FN-silk controls. The reduced adhesion reported here would therefore likely reduce the risk of colonization under the conditions upon implantation.

Another approach could be to combine the dual-functional silks used herein with other variants of bioactive silk proteins,

DOI: 10.1021/acsami.9b05531
ACS Appl. Mater. Interfaces 2019, 11, 24999−25007

for example, by mixing DspB-FN-silk with recombinant silk fused with growth factors[14] or substances that could regulate the polarization of macrophages to achieve better tissue integration and healing. It is indeed interesting to construct multifunctional coatings also with different types of antimicrobials. For example, DNaseI has previously been shown efficient in inhibiting biofilm formation when immobilized on poly(methyl methacrylate) surfaces using dopamine activation, in a study similar to this.[38] Other deoxyribonucleases, proteases, and glycosidases have been suggested for dispersal of biofilms and are relevant candidates for functionalization of silk coatings.[9,39]

Previous reports on the ability of 4RepCT silk to assemble into coatings on various material types such as silicon dioxide, titanium, stainless steel, and hydroxyapatite depict its versatility.[11,40] By expanding the toolbox for functionalization with bioactive domains under physiological-like conditions using sortase-mediated protein conjugation as presented here, further possibilities can be explored, such as construction of multifunctional silk coatings also for soft implants, to display a combination of peptides, protein domains, and enzymes on the surface that can stimulate inflammatory responses toward improved healing and tissue regeneration.

CONCLUSIONS

Silk coatings conjugated with the biofilm-dispersal enzyme DspB or the endolysins SAL-1 or PlySs2, respectively, showed reduced bacterial adhesion compared with $silk_{wt}$ and FN-silk coatings. Since the adhered bacteria were still viable, the main effect of the immobilized enzymes seems to be to prevent adhesion rather than lyse the bacteria. A large proportion of the bacteria seen on the silk coatings functionalized with enzymes were mobile, in contrast to the firm adhesion observed on FN-silk and $silk_{wt}$ coatings. The mobile bacteria could be washed off more easily. Thus, the silk coatings with conjugated enzymes may be used to allow easier removal of bacteria in applications where bacterial colonization needs to be reduced. In addition, silk coatings of FN-silk, SAL-1-FN-silk, PlySs2-FN-silk, and DspB-FN-silk showed excellent adhesion, viability, and growth of osteoblast-like U-2 OS cells both during the first hour of adhesion and during week-long culturing. The dual-functional silk coatings are envisioned to be suitable for application onto a wide range of biomaterials to allow cells from the surrounding tissue to adhere faster than bacteria. In this way, it would support the cells in winning the race to the surface and obtain successful tissue integration as well as prevention of biomaterial-associated infection.

ASSOCIATED CONTENT

Supporting Information

The Supporting Information is available free of charge on the ACS Publications website at DOI: 10.1021/acsami.9b05531.

SDS-PAGE analysis of produced proteins, evaluation of the catalytic activities of SAL-1 and PlySs2 in solution, and evaluation of the catalytic activity of immobilized DspB compared with DspB in solution (PDF)

Time-lapse capture of PlySs2 on $silk_{wt}$ (MPG)

Time-lapse capture of $silk_{wt}$ control (MPG)

AUTHOR INFORMATION

Corresponding Author

*E-mail: myh@kth.se.

ORCID

My Hedhammar: 0000-0003-0140-419X

Present Address

⊥BioGaia AB, P.O. Box 3242, SE-103 64 Stockholm, Sweden (H.B.).

Notes

The authors declare the following competing financial interest(s): M.H. has shares in Spiber Technologies AB, a company that aims to commercialize recombinant spider silk.

ACKNOWLEDGMENTS

We thank Spiber Technologies AB for providing silk proteins. A special thanks to Kristina Westerlund for kindly providing the Sortase A* construct and valuable guidance. Rajeev Pasupuleti and Oskar Öhman are gratefully acknowledged for help in purifying Sortase A* and the enzymes. Thanks to Fredrik Seijsing who performed the turbidity reduction assays. Sincere gratitude to Ed D. Jong for providing counting scripts for the micrographs. Formas, Swedish Research Council, Knut and Alice Wallenbergs stiftelse, and Gålöstiftelsen are acknowledged for funding.

REFERENCES

(1) Busscher, H. J.; van der Mei, H. C.; Subbiahdoss, G.; Jutte, P. C.; van den Dungen, J. J. A. M.; Zaat, S. A. J.; Schultz, M. J.; Grainger, D. W. Biomaterial-Associated Infection: Locating the Finish Line in the Race for the Surface. *Sci. Transl. Med.* **2012**, *4*, No. 153rv10.

(2) Donlan, R. M.; Costerton, J. W. Biofilms: Survival Mechanisms of Clinically Relevant Microorganisms. *Clin. Microbiol. Rev.* **2002**, *15*, 167−193.

(3) Stewart, P. S.; Costerton, J. W. Antibiotic Resistance of Bacteria in Biofilms. *Lancet* **2001**, *358*, 135−138.

(4) World Health Organization. *Antimicrobial Resistance*; WHO Fact sheets 194, 2014.

(5) Li, B.; Webster, T. J. Bacteria Antibiotic Resistance: New Challenges and Opportunities for Implant-Associated Orthopedic Infections. *J. Orthop. Res.* **2018**, 22−32.

(6) Zimmerli, W.; Sendi, P. Orthopaedic Biofilm Infections. *APMIS* **2017**, *125*, 353−364.

(7) Hickok, N. J.; Shapiro, I. M. Immobilized Antibiotics to Prevent Orthopaedic Implant Infections. *Adv. Drug Delivery Rev.* **2012**, *64*, 1165−1176.

(8) Bazaka, O.; Bazaka, K. Surface Modification of Biomaterials for Biofilm Control. In *Biomaterials and Medical Device—Associated Infections*; Elsevier, 2015; pp 103−132.

(9) Fleming, D.; Rumbaugh, K. Approaches to Dispersing Medical Biofilms. *Microorganisms* **2017**, *5*, 15.

(10) Mas-Moruno, C.; Su, B.; Dalby, M. J. Multifunctional Coatings and Nanotopographies: Toward Cell Instructive and Antibacterial Implants. *Adv. Healthcare Mater.* **2018**, No. 1801103.

(11) Nilebäck, L.; Hedin, J.; Widhe, M.; Floderus, L. S.; Krona, A.; Bysell, H.; Hedhammar, M. Self-Assembly of Recombinant Silk as a Strategy for Chemical-Free Formation of Bioactive Coatings: A Real-Time Study. *Biomacromolecules* **2017**, *18*, 846−854.

(12) Widhe, M.; Shalaly, N. D.; Hedhammar, M. A Fibronectin Mimetic Motif Improves Integrin Mediated Cell Biding to Recombinant Spider Silk Matrices. *Biomaterials* **2016**, *74*, 256−266.

(13) Johansson, U.; Ria, M.; Åvall, K.; Shalaly, N. D.; Zaitsev, S. V.; Berggren, P.-O.; Hedhammar, M. Pancreatic Islet Survival and Engraftment Is Promoted by Culture on Functionalized Spider Silk Matrices. *PLoS One* **2015**, *10*, No. e0130169.

(14) Thatikonda, N.; Nilebäck, L.; Kempe, A.; Widhe, M.; Hedhammar, M. Bioactivation of Spider Silk with Basic Fibroblast Growth Factor for in Vitro Cell Culture: A Step toward Creation of Artificial ECM. *ACS Biomater. Sci. Eng.* **2018**, *4*, 3384−3396.

(15) Jansson, R.; Thatikonda, N.; Lindberg, D.; Rising, A.; Johansson, J.; Nygren, P.-Å.; Hedhammar, M. Recombinant Spider Silk Genetically Functionalized with Affinity Domains. *Biomacromolecules* **2014**, *15*, 1696−1706.
(16) Altai, M.; Westerlund, K.; Velletta, J.; Mitran, B.; Honarvar, H.; Karlström, A. E. Evaluation of Affibody Molecule-Based PNA-Mediated Radionuclide Pretargeting: Development of an Optimized Conjugation Protocol and 177 Lu Labeling. *Nucl. Med. Biol.* **2017**, *54*, 1−9.
(17) Schmelcher, M.; Donovan, D. M.; Loessner, M. J. Bacteriophage Endolysins as Novel Antimicrobials. *Future Microbiol.* **2012**, *7*, 1147−1171.
(18) Roach, D. R.; Donovan, D. M. Antimicrobial Bacteriophage-Derived Proteins and Therapeutic Applications. *Bacteriophage* **2015**, *5*, No. e1062590.
(19) Czaplewski, L.; Bax, R.; Clokie, M.; Dawson, M.; Fairhead, H.; Fischetti, V. A.; Foster, S.; Gilmore, B. F.; Hancock, R. E. W.; Harper, D.; Henderson, I. R.; Hilpert, K.; Jones, B. V.; Kadioglu, A.; Knowles, D.; Ólafsdóttir, S.; Payne, D.; Projan, S.; Shaunak, S.; Silverman, J.; Thomas, C. M.; Trust, T. J.; Warn, P.; Rex, J. H. Alternatives to Antibiotics - a Pipeline Portfolio Review. *Lancet Infect. Dis.* **2016**, *16*, 239−251.
(20) Gilmer, D. B.; Schmitz, J. E.; Euler, C. W.; Fischetti, V. A. Novel Bacteriophage Lysin with Broad Lytic Activity Protects against Mixed Infection by Streptococcus Pyogenes and Methicillin-Resistant *Staphylococcus aureus*. *Antimicrob. Agents Chemother.* **2013**, *57*, 2743−2750.
(21) Gilmer, D. B.; Schmitz, J. E.; Thandar, M.; Euler, C. W.; Fischetti, V. A. The Phage Lysin PlySs2 Decolonizes *Streptococcus suis* from Murine Intranasal Mucosa. *PLoS One* **2017**, *12*, No. e0169180.
(22) Jun, S. Y.; Jang, I. J.; Yoon, S.; Jang, K.; Yu, K.-S.; Cho, J. Y.; Seong, M.-W.; Jung, G. M.; Yoon, S. J.; Kang, S. H. Pharmacokinetics and Tolerance of the Phage Endolysin-Based Candidate Drug SAL200 after a Single Intravenous Administration among Healthy Volunteers. *Antimicrob. Agents Chemother.* **2017**, *61*, No. e02629-16.
(23) Kaplan, J. B.; Ragunath, C.; Ramasubbu, N.; Fine, D. H. Detachment of *Actinobacillus Actinomycetemcomitans* Biofilm Cells by an Endogenous -Hexosaminidase Activity. *J. Bacteriol.* **2003**, *185*, 4693−4698.
(24) Itoh, Y.; Wang, X.; Hinnebusch, B. J.; Preston, J. F.; Romeo, T. Depolymerization of -1,6-N-Acetyl-D-Glucosamine Disrupts the Integrity of Diverse Bacterial Biofilms. *J. Bacteriol.* **2005**, *187*, 382−387.
(25) Widhe, M.; Johansson, U.; Hillerdahl, C.-O.; Hedhammar, M. Recombinant Spider Silk with Cell Binding Motifs for Specific Adherence of Cells. *Biomaterials* **2013**, *34*, 8223−8234.
(26) Tasiopoulos, C. P.; Widhe, M.; Hedhammar, M. Recombinant Spider Silk Functionalized with a Motif from Fibronectin Mediates Cell Adhesion and Growth on Polymeric Substrates by Entrapping Cells During Self-Assembly. *ACS Appl. Mater. Interfaces* **2018**, *10*, 14531−14539.
(27) Stark, M.; Grip, S.; Rising, A.; Hedhammar, M.; Engström, W.; Hjälm, G.; Johansson, J. Macroscopic Fibers Self-Assembled from Recombinant Miniature Spider Silk Proteins. *Biomacromolecules* **2007**, *8*, 1695−1701.
(28) Chen, I.; Dorr, B. M.; Liu, D. R. A General Strategy for the Evolution of Bond-Forming Enzymes Using Yeast Display. *Proc. Natl. Acad. Sci. U.S.A.* **2011**, *108*, 11399−11404.
(29) Jun, S. Y.; Jung, G. M.; Son, J.-S.; Yoon, S. J.; Choi, Y.-J.; Kang, S. H. Comparison of the Antibacterial Properties of Phage Endolysins SAL-1 and LysK. *Antimicrob. Agents Chemother.* **2011**, *55*, 1764−1767.
(30) Nilebäck, L.; Arola, S.; Kvick, M.; Paananen, A.; Linder, M. B.; Hedhammar, M. Interfacial Behavior of Recombinant Spider Silk Protein Parts Reveals Cues on the Silk Assembly Mechanism. *Langmuir* **2018**, *34*, 11795−11805.
(31) Nilebäck, L. Expanded Knowledge on Silk Assembly for Development of Bioactive Silk Coatings. Doctoral dissertation TRITA-CBH-FOU-2019:9; KTH Royal Institute of Technology, 2019.
(32) Henderson, B.; Nair, S.; Pallas, J.; Williams, M. A. Fibronectin: A Multidomain Host Adhesin Targeted by Bacterial Fibronectin-Binding Proteins. *FEMS Microbiol. Rev.* **2011**, *35*, 147−200.
(33) Schröder, A.; Schröder, B.; Roppenser, B.; Linder, S.; Sinha, B.; Fässler, R.; Aepfelbacher, M. *Staphylococcus Aureus* Fibronectin Binding Protein-A Induces Motile Attachment Sites and Complex Actin Remodeling in Living Endothelial Cells. *Mol. Biol. Cell* **2006**, *17*, 5198−5210.
(34) Song, L.; Hou, J.; van der Mei, H. C.; Veeregowda, D. H.; Busscher, H. J.; Sjollema, J. Antimicrobials Influence Bond Stiffness and Detachment of Oral Bacteria. *J. Dent. Res.* **2016**, *95*, 793−799.
(35) Gristina, A. G. Biomaterial-Centered Infection: Microbial Adhesion versus Tissue Integration. *Science* **1987**, *237*, 1588−1595.
(36) Subbiahdoss, G.; Kuijer, R.; Grijpma, D. W.; van der Mei, H. C.; Busscher, H. J. Microbial Biofilm Growth vs. Tissue Integration: "The Race for the Surface" Experimentally Studied. *Acta Biomater.* **2009**, *5*, 1399−1404.
(37) Wiegand, C.; Abel, M.; Ruth, P.; Hipler, U.-C. HaCaT Keratinocytes in Co-Culture with *Staphylococcus Aureus* Can Be Protected from Bacterial Damage by Polihexanide. *Wound Repair Regener.* **2009**, *17*, 730−738.
(38) Swartjes, J. J.; Das, T.; Sharifi, S.; Subbiahdoss, G.; Sharma, P. K.; Krom, B. P.; Busscher, H. J.; van der Mei, H. C. A Functional DNase I Coating to Prevent Adhesion of Bacteria and the Formation of Biofilm. *Adv. Funct. Mater.* **2013**, *23*, 2843−2849.
(39) Kaplan, J. B. Biofilm Dispersal: Mechanisms, Clinical Implications, and Potential Therapeutic Uses. *J. Dent. Res.* **2010**, *89*, 205−218.
(40) Horak, J.; Jansson, R.; Dev, A.; Nilebäck, L.; Behnam, K.; Linnros, J.; Hedhammar, M.; Karlström, A. E. Recombinant Spider Silk as Mediator for One-Step, Chemical-Free Surface Biofunctionalization. *Adv. Funct. Mater.* **2018**, *28*, No. 1800206.

DOI: 10.1021/acsami.9b05531
ACS Appl. Mater. Interfaces 2019, 11, 24999−25007